Nanoscale

Accepted Manuscript

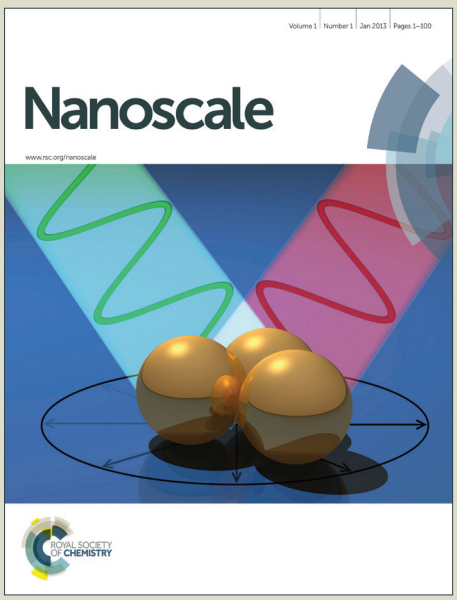

ROYAL SOCIETY OF CHEMISTRY

www.rsc.org/nanoscale

Tridentate Benzylthiols on Gold(111): Control of Self-Assembly Geometry

Mohamed A. Mezour, Iryna I. Perepichka[†], Oleksandr Ivasenko[‡], R. Bruce Lennox, Dmitrii F. Perepichka**

Department of Chemistry and Centre for Self-Assembled Chemical Structures, McGill University, 801 Sherbrooke St. West, Montreal (QC) H3A 0B8, Canada

ABSTRACT

A set of hexasubstituted benzene derivatives with three thiol groups in the 1, 3, 5 positions and varied alkyl substituents in the 2, 4, 6 positions (**Me_3-BTMT**, **Et_3-BTMT**, **ODe_3-BTMT)** has been synthesized and self-assembled on Au(111). The resulting self-assembled monolayers (SAMs) are characterized by scanning tunneling microscopy (STM), X-ray photoelectron spectroscopy (XPS), and electrochemistry. The molecular orientation and long-range order are affected by the "gear effect" of the hexasubstituted benzene ring and van der Waals interactions between the physisorbed alkyl chains drive. **Me_3-BTMT** adopts a standing up orientation which results in a high molecular areal density but also the lowest degree of chemisorption (1 to 2 Au-S bonds per molecule). In contrast, **Et_3-BTMT** favors a lying down orientation with a greater number of surface-bonded thiol groups (2 to 3) per molecule which is due to the preferred all-"anti" conformation of this molecule. Finally, **ODe_3-BTMT** adsorbs mainly in a lying down orientation, forming the SAM with the highest degree of chemisorption (all thiol groups are gold-bonded) and the lowest molecular areal density.

INTRODUCTION

Thiol-based self-assembled monolayers have been widely used to tailor the interfacial properties of gold and other metals for applications in diverse fields such as corrosion inhibition,[1] organic and molecular electronic devices,[2,3,4] switches,[5,6] biomolecular adhesion,[7] chemosensors,[8,9] and biosensors.[10]

A number of these applications depend on the long-term stability of the component.[11] Although the Au-S gold bond is moderate in strength (38–48 kcal/mol),[12] formation of a disulphide bond by the departing ligands provides an energetically feasible desorption mechanism.[13] In thiol-free solution thiol-based SAMs can desorb to a significant extent within a few days.[14] In the presence of air the desorption is further facilitated by oxidation of the thiol groups.[15]

Several strategies have been employed to enhance SAMs stability, by strengthening the molecule-substrate interactions and/or the lateral interactions between adsorbates. The use of multidentate ligands with several anchoring thiol groups is one of the most effective methods for generating SAMs with long-term stability.[16,17] Such an approach has been successfully employed using different molecular architectures, as illustrated in Figure 1.[18,19,20,21,22,23,24,25,26,27]

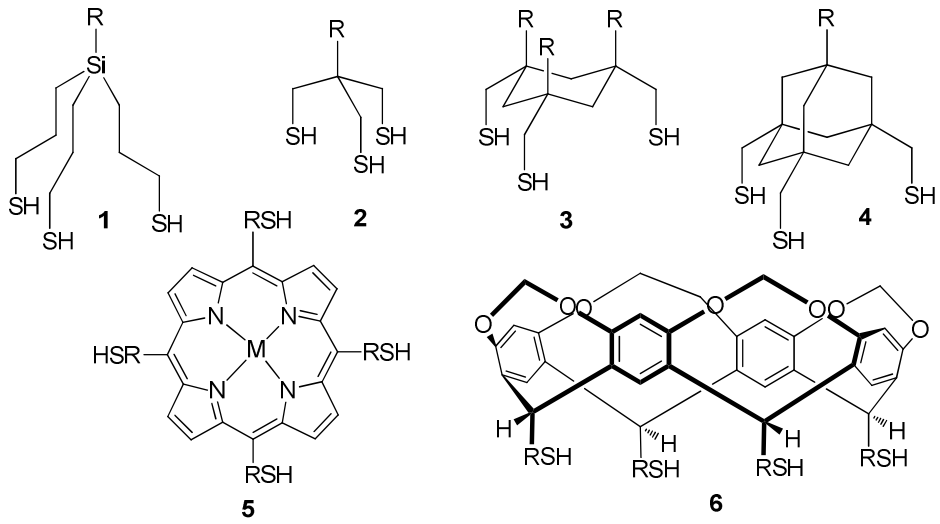

Fig. 1. Examples of multidentate thiols in SAM research.

These multidentate thiols are frequently applied in design of functional SAMs, in molecular electronics and related applications.[28,29,30,31] For example, **1** and **2** motifs have been used for carrying various functional units, including large (bio)macromolecules: fluophores,[32] porphyrins,[29] fullerenes,[30] DNA,[33] etc. However, controlling molecular orientation in multidentate thiols is often difficult and the resulting SAMs are generally much less ordered than those based on monodentate thiol.[21] An incomplete bonding of the thiol groups has been shown by X-ray photoelectron spectroscopy (XPS) in many cases for **1** and **2**.[34,35] In the case of porphyrin tetrathiol derivatives **5**, only one or two thiol groups are typically attached to the gold surface.[26,36,37] This is often detrimental not only for the stability but also

for the order of the SAM, as having the "free" thiol group makes the SAM vulnerable to multilayer formation (through disulfide cross-links), oxidation, and other defects. The uncontrolled molecular orientation affects the desired functional characteristics of the SAMs; eg, the impossibility of achieving flat-lying fully bonded conformation in case of porphyrin **5** negatively impacts the photo-electrochemical and electro-catalytic properties of its SAMs.[26,36,37] Together with the slower dynamics of the multidentate thiol, such partial binding might also be responsible for the lower lateral order in their SAMs. A significant control of the molecular orientation was, nevertheless, achieved using rigid non-aromatic adamantane and cyclohexane cores **(3** and **4)** which can provide complete Au-S bonding and long-range order in the SAMs.[22,25]

In this work, we explore a new, synthetically versatile, molecular motif of tridentate thiols suitable for formation of SAMs. Such design, based on a single rigid aromatic core with three "legs" is advantageous for at least four reasons. First, it allows controlling molecular conformation by exploiting the steric gearing and conformational constraints of the hexasubstituted benzene.[38] Second, the desorption pathways involving the formation of disulfides are disfavored due to the rigidity of the aromatic ring.[39] Third, the flat-lying aromatic ring allows to dramatically reduce the thickness (~0.5 nm) of the monolayer comparing to any other thiol-based SAMs, which should lead to enhanced electronic interactions of the surface with the environment (electron tunneling, sensing, *etc*). Finally, intermolecular interactions of substituents on the benzene core (*eg*, long alkyl chains) could allow tuning the lateral structure/periodicity of the monolayer, merging aspects of the fields of chemisorbed SAMs and self-assembled molecular networks (SAMNs).[40,41,42]

Herein, we report three new tridentate benzenetris(methylthiols) (BTMT), substituted with methyl, ethyl and decyloxy groups (**Me_3-BTMT**, **Et_3-BTMT**, **ODe_3-BTMT**) (Fig. 2) and explore their self-assembly behavior on Au(111) surface. A comparative characterization of these SAMs, carried out using XPS, electrochemistry, and STM, provides insight into their relative SAM formation properties.

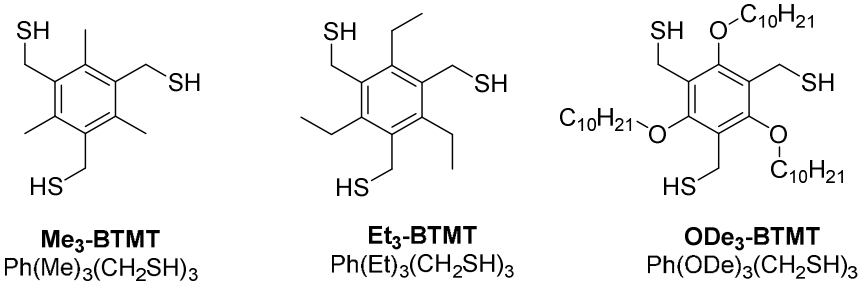

Me_3-BTMT
$Ph(Me)_3(CH_2SH)_3$

Et_3-BTMT
$Ph(Et)_3(CH_2SH)_3$

ODe_3-BTMT
$Ph(ODe)_3(CH_2SH)_3$

Fig. 2. Structure of tridentate benzylthiols.

RESULTS AND DISCUSSION

Hexasubstituted benzene derivatives have been widely used as synthetically accessible scaffolds for building molecular hosts in supramolecular systems.[38,43,44] Conformational control in this system results from the pre-organized *syn*-geometry of substituents in 1, 3, 5 (as well as 2, 4, 6) positions brought about by a thermodynamic preference for an *anti* orientation of the neighboring substituents, which minimizes steric interactions.[45] While such preorganization has been extensively exploited in supramolecular templates, to our knowledge no studies on its use in molecular self-assembly on surfaces have been reported. We speculated that such conformational control might improve the ordering in tridentate SAMs by forcing the orientation of each thiol anchor toward the surface. Accordingly, we have synthesized three new benzenetris(methylthiols) with three alkyl groups (methyl, ethyl, and decyloxy) substituents (Scheme 1 and SI).

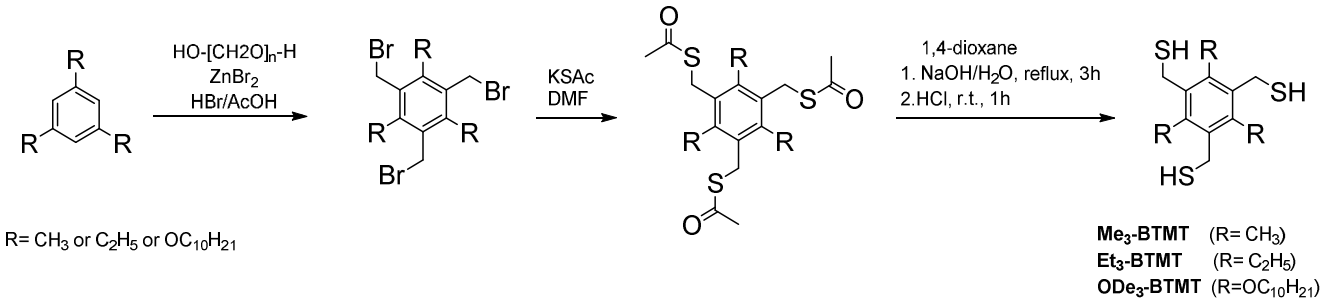

Scheme 1. Synthesis of tridentate benzylthiols.

Density functional theory (DFT) calculations at the B3LYP/6-31G(d) level were performed on **Me$_3$-BTMT**, **Et$_3$-BTMT** and **ODe$_3$-BTMT** to evaluate the energetic preference for the *syn* vs *anti* conformation (Fig. 3). For **Me$_3$-BTMT**, the *anti* conformation (with thiol groups on the opposite side of the ring) is slightly preferred by 0.9 kcal/mol, which is likely due to weak dipole-dipole interactions of the thiol groups. In contrast **Et$_3$-BTMT** shows a preference of the *syn* conformer by 2.2 kcal/mol, in where the steric repulsion with the bulkier ethyl groups is minimized. This corresponds to ca. 99% of molecules adopting the *syn* conformation at room temperature. For **ODe$_3$-BTMT**, the difference between *syn* and *anti* conformers is extremely small (~0.6 kcal/mol). We note that even for **Et$_3$-BTMT** the calculated preference of the *syn* conformer is more than an order of magnitude smaller than the expected energy of chemisorption. However, this does not make it inconsequential, since the difference between *lying down* and *standing up* chemisorption geometries are also much smaller than the total adsorption energy. Furthermore, an interconversion barrier between *syn* and *anti* conformers (~12 kcal/mol for **Et$_3$-BTMT**, Fig. SI3) might provide kinetic preference for the *lying down* geometry with three Au-S bonds.

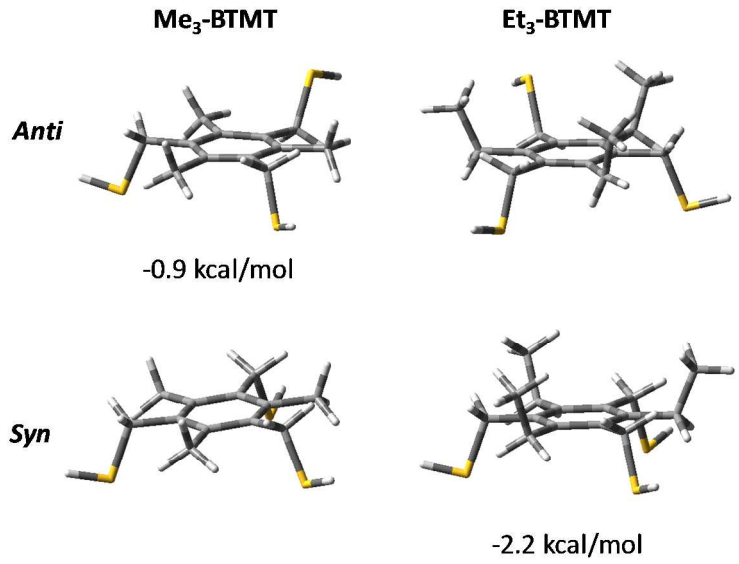

Fig. 3. Relative stabilization energies (B3LYP/6-31G(d)) of *syn* and *anti* conformations of **Me_3-BTMT** and **Et_3-BTMT**. *Syn*/*anti* refers to the orientation of one CH_2SH group relative to the other two.

STM characterization

STM provides direct insights into local structures of molecular monolayers on conductive surfaces and has been frequently used for the analysis of thiol assemblies on Au(111).[46] STM images of **Me_3-BTMT** and **Et_3-BTMT** SAMs (Fig. 4) exhibit rather disordered structures, as compared to the 2D crystalline SAMs (Fig. SI1) formed under identical conditions by 1-octanethiol (**C_8SH)**, used as a reference throughout this study. A partial ordering is, however, manifested as rows of bright protrusion, particularly for **Me_3-BTMT.** The separation between these rows (~1.3 nm) corresponds well to the lateral size of the molecule plus the van der Waals (vdW) spacing (Fig. SI2). Although 2D FFT (Fig. 4g) shows a weak indication of long-range ordering, the quality of the data does not allow extracting reliable unit cell parameters. Therefore, a pair correlation analysis of the observed bright protrusions has been performed via the nearest three-point contacts (Fig. SI4). This procedure provides both the average intermolecular distances and the relative orientation of two contacts emanating from the same origin (an angle of a "local unit cell"). The resulting histograms of the nearest neighbor distances for **Me_3-BTMT** shows a bimodal distribution with preferred distances at ~0.5 nm and ~1.2 nm (Fig. 4c). The longer of the two distances corresponds to the separation between the aforementioned rows, while the shorter one can be attributed to the preferentially spacing along the rows. The latter is significantly smaller than the lateral size of the molecules in a *lying down* orientation on the surface. However, it is consistent with the molecules *standing up* and closely packed in the rows of co-aligned benzene rings, with possible π-stacking interaction (Fig. 4e).

The pair correlation analysis[47,48] (see also Fig. SI4) for the SAM of **Et_3-BTMT** (Fig. 4d) shows the most frequently observed intermolecular contacts at ~1.0 nm which is consistent with the tentative model of flat-lying molecules (Fig. 4f). A minor peak at ~0.6 nm in the distribution histogram suggests some occurrence of vertically oriented molecules, as tentatively presented by the model in Fig. 4h. Thus, the discussed above conformational effect of the ethyl groups and the possible hindrance to π-stacking of the vertically oriented molecules seem to favor, albeit not fully enforce, the *lying down* assembly of the **Et_3-BTMT**. A co-existence of the two self-assembly modes may well be responsible for the generally less-ordered STM appearance of the **Et_3-BTMT** SAM.

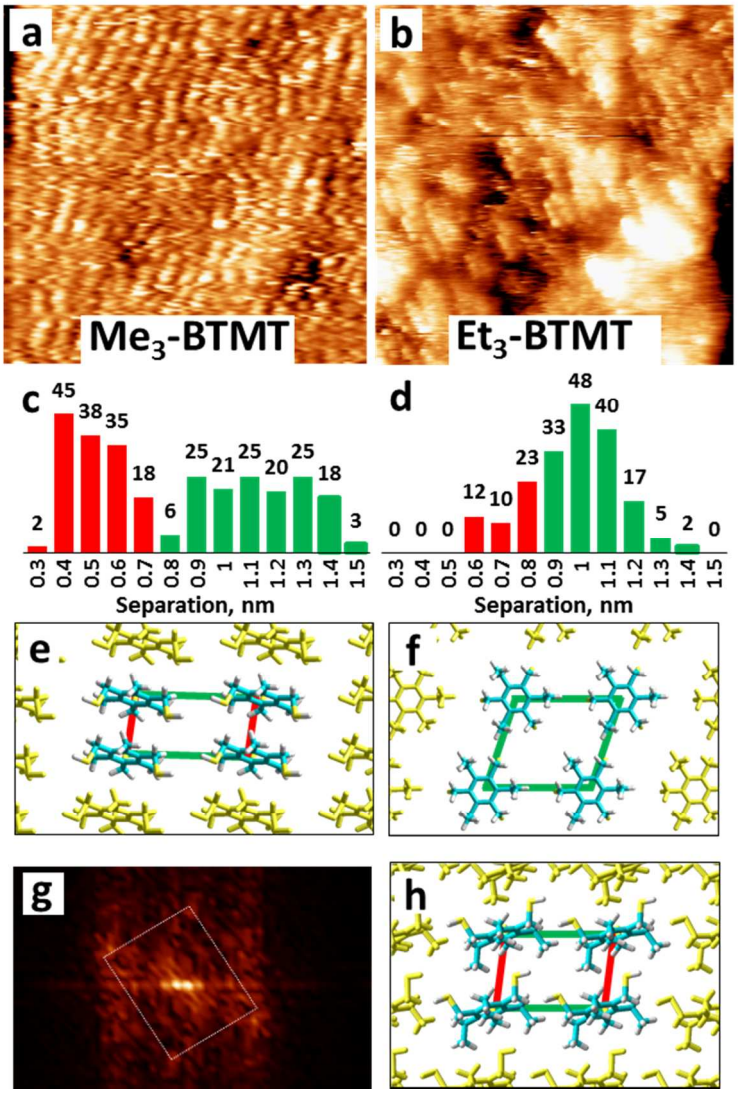

Fig. 4. Representative 25×25 nm STM images of SAMs formed by **Me_3-BTMT** (a) and **Et_3-BTMT** (b); scanning parameters: (a) V_t = 800 mV, I_t = 0.2 nA; (e) V_t = 600 mV, I_t = 0.3 nA). (c), (d) Corresponding histograms of the nearest neighbor distances; the red bars correspond to intermolecular separations that are only possible for *standing up* molecules; green bars represent distances at which the neighboring molecules can either lie down or stand up on the surface. Tentative models for close-packed assembly of '*standing up*' **Me_3-BTMT** (e) and **Et_3-BTMT** (h) and '*lying down*' **Et_3-BTMT** (f). (g) Fast Fourier transform (FFT) image of (a).

To further promote the *lying down* orientation, the trithiol **ODe$_3$-BTMT** was equipped with three long dodecyl chains which were expected to engage in multiple van der Waals interactions with the surface and between themselves. Fig. 5 shows STM images of SAMs of **ODe$_3$-BTMT** and of its non-thiolated analog **ODe$_3$-B**. The defining role of the alkyl chain interactions is apparent from the assembly of **ODe$_3$-B** which forms a well-ordered 2D periodic lattice with an oblique unit cell (a = 1.4 ± 0.1 nm; b = 2.3 ± 0.2 nm; α = 78 ± 6°). The high-resolution image of this assembly clearly shows the orientation of the alkyl chains (Fig. 5c). Measurements of the area available for adsorption of alkyl side chains, together with the number of visualized alkyl chains, suggest that two interdigitated alkyl chains are adsorbed on the surface, while the third one protrudes into the solution (as observed earlier for similar molecules).[49]

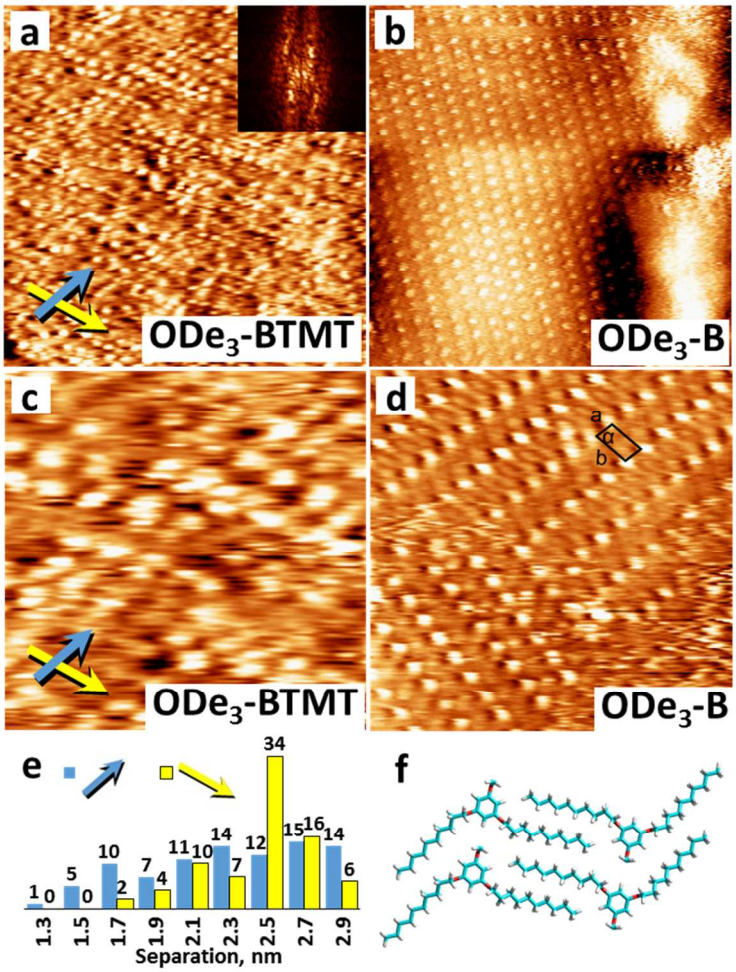

Fig. 5. Representative STM images of SAMs formed by **ODe$_3$-BTMT** (a,c) and **ODe$_3$-B** (b,d). Image size and scanning parameters: (a) 77×77 nm, V_b = 300 mV, I_t = 0.15 nA; (b) 40×40 nm, V_b = 800 mV, I_t = 0.08 nA; (c) 25×25 nm, V_b = 300 mV, I_t = 0.15 nA; (d) 25×25 nm, V_b = 800 mV, I_t = 0.08 nA. An inset in (a) shows fast Fourier transform (FFT) image of the STM micrograph. (e) A histograms of the nearest neighbor distance of **ODe$_3$-BTMT** along (yellow bars) and across (blue bars) the apparent one-dimensional rows (marked with the yellow arrow in (a) and (c). (f) Tentative models for self-assembly of **ODe$_3$-B**. For clarity, the alkyl chains pointing into the solution face are not shown.

The SAM of the corresponding trithiol **ODe$_3$-BTMT** is significantly less ordered than that of the physisorbed **ODe$_3$-B**, and contrary to **Me$_3$-BTMT** and **Et$_3$-BTMT**, there are no sub-nanometer nearest neighbor separation in **ODe$_3$-BTMT**. The average three-point contact (a=1.7±0.5 nm, b=2.5±0.5 nm, α =75°±20°, Fig. SI4) is similar but slightly larger than the unit cell parameters of the parent **ODe$_3$-B** suggesting a similar adsorption geometry.

XPS characterization of tridentate benzylthiols

XPS has been widely used for the characterization of thiol-based SAMs. The binding energy (BE) of the S2p signal provides clear evidence for S-Au bond formation. XPS S2p spectra of the **C$_8$SH**, **Me$_3$-BTMT, Et$_3$-BTMT** and **ODe$_3$-BTMT** SAMs are presented in Fig. 6. Consistent with the literature, the S2p spectrum of C_8SH shows a well resolved doublet with a BE of 162.0 eV ($S2p_{3/2}$ peak).[50] The **Me$_3$-BTMT, Et$_3$-BTMT** and **ODe$_3$-BTMT** SAMs show broad S2p peaks best fitted as two doublets at 162.0 eV and 163.0 eV (for $S2p_{3/2}$ peaks) assigned to Au-bonded and non-bonded sulphur, respectively. No oxidized sulphur is detected at higher binding energy values (>166 eV[50]).

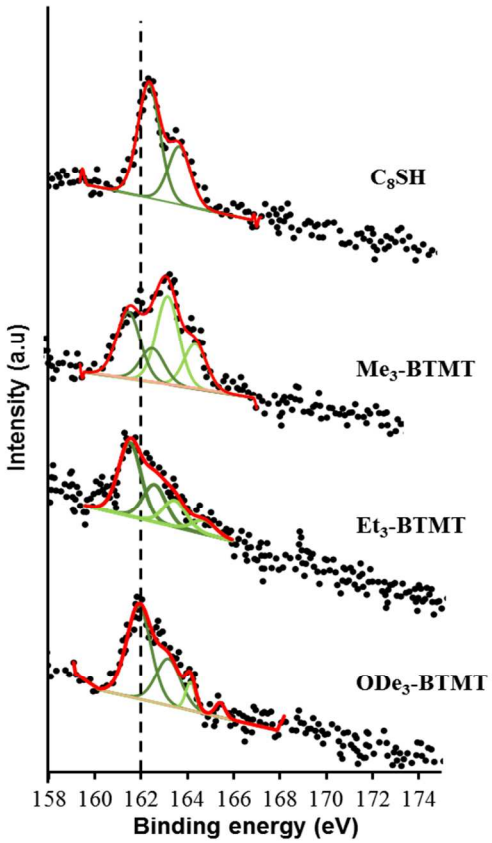

Fig. 6. X-ray photoelectron spectra and their deconvoluted components of the four SAMs studied, formed by 18 h immersion of Au/mica slides in 0.1mM DMF solutions of the corresponding thiols.

Compared to the SAM of **C_8SH,** where all sulphurs are bound to gold (100%), the trithiols reveal a mixture of bonded and nonbonded sulphur (Table 1). The lowest degree of sulphur binding (~44%) was observed for **Me_3-BTMT**, while **Et_3-BTMT** and **ODe_3-BTMT** shows a higher bound/non-bound thiol with the values of ~73% and ~90% respectively.

Table 1. A summary of XPS and electrochemical analysis of **C_8SH**, **Me_3-BTMT, Et_3-BTMT** and **ODe_3-BTMT** SAMs on Au.

		C_8SH	**Me_3-BTMT**	**Et_3-BTMT**	**ODe_3-BTMT**
S_b/S_T (%)[a]		100	44	73	90
S_T/Au[b]		4.2×10^{-3}	7.5×10^{-3}	5.6×10^{-3}	4.2×10^{-3}
Cycle 1	E[c] (V vs Ag/AgCl)	−0.88	−0.83	−0.86	−1
	Q_c ($\mu C/cm^2$)[d]	33.1	31.6	24.2	14.5
	Γ (mol/cm^2)[e]	3.4×10^{-10}	2.6×10^{-10}	1.1×10^{-10}	0.6×10^{-10}
	A' (nm^2)[f]	0.5	0.7	1.6	2.8
	fwhm (mV)[g]	37	46	113	120
Cycle 2	E_{red} (V vs Ag/AgCl)	−0.84	−0.85	−0.89	−0.92
	Q_c ($\mu C/cm^2$)	15.4	13.9	11.8	13.6
	Q_{c2}/Q_{c1}	0.47	0.44	0.49	0.94

(a) XPS ratio of bound sulfur to total sulfur (b) XPS ratio of total sulfur to gold (c) desorption peak potential, (d) desorption charge density, (e) electrochemical surface concentration, (f) area per molecule (deduced from Γ), and (g) full width at half-maximum of a desorption wave.

The ratio of the peak area of bound/non-bound sulphur might be related to the conformation of tridentate molecules forming the SAMs. The observed ratio suggests that **Me_3-BTMT** molecules are most likely attached to the gold substrate in a standing-up configuration, which allows for only one of three thiol groups to bind to the surface. On the other hand, **Et_3-BTMT** involves both the lying down and standing-up conformations, resulting in ca. two thiol groups per molecule being bound to the gold surface. This difference can be explained by the energetic preference of all thiol groups in **Et_3-BTMT** to adopt the *syn* conformation (Fig. 3), which facilitates their binding with the surface. In addition, the bulkier ethyl substituents can inhibit the $\pi\ldots\pi$ interactions between the aromatic cores that are the likely source of stabilization of the standing-up conformation of the **Me_3-BTMT** case, as suggested by STM measurements.

Interestingly, **ODe$_3$-BTMT** does not show a large preference for the co-facial *syn* position of its thiol groups, and exhibits the lowest extent of non-bound sulphur. This most likely should be attributed to the large preference of these molecules to adsorb in a lying down orientation on the surface, so as to maximize the vdW interactions of the alkoxy chains with the gold and between themselves.

The analysis of the ratio of the S2p and Au4f peak intensity (Table 1) shows a decrease of the molecular surface density upon changing the size of a substituent from Me to Et to ODe. This trend is also in agreement with the footprint of the different conformations of these tridentate molecules. Indeed, **ODe$_3$-BTMT** shows the lowest surface density, followed by **Et$_3$-BTMT** (both in a lying down conformation) and finally **Me$_3$-BTMT** which adopts standing-up conformation. For **C$_8$SH**, the lower sulfur to gold ratio could be explained by attenuation of the photoelectrons by standing up alkyl chain (which leads to a relative enhancement of the Au signal from defective areas of the SAM[51]).

Electrochemical desorption of tridentate benzylthiols

Further information concerning the strength of the intermolecular interaction, degree of molecular order, and surface density of SAMs was acquired by electrochemical desorption experiments. Fig. 7 shows consecutive cyclic voltammograms (CV) of **C$_8$SH**, **Me$_3$-BTMT, Et$_3$-BTMT** and **ODe$_3$-BTMT** coated gold electrodes. The CVs were recorded by repetitive scanning of the potential of the SAM-modified gold electrode from 0 to –1.3 V at 0.02 V/s in aqueous KOH solution (0.5 M). On cathodic sweep, all SAMs exhibit an irreversible reduction wave between E_{red} −0.83 and −1 V vs Ag/AgCl indicative of S–Au bond cleavage.[52] Significant differences in the shape and position of the desorption peaks as well as the quantity of reductive charge for the four SAMs were observed (Table 1).

The shape and the location of the desorption peak is strongly affected by the state of the monolayer, including factors such as the packing density and the magnitude of the lateral interactions between the adsorbed molecules.[53,54] As shown in Fig. 7, desorption of a **C$_8$SH** SAM results in a narrow symmetric cathodic peak at –0.88 V. With respect to the **C$_8$SH** SAM, the reduction peaks of **Me$_3$-BTMT, Et$_3$-BTMT** SAMs were observed at less negative potentials, at –0.83 V and –0.86 V, respectively, while **ODe$_3$-BTMT** SAM reveals a peak at a more negative potential (around –1 V). The shift toward more negative potential was previously correlated with the electrochemical stability of the SAM.[53] The following trend in SAM stability is thus suggested: **ODe$_3$-BTMT** > **C$_8$SH** > **Et$_3$-BTMT** > **Me$_3$-BTMT**. The apparent electrochemical stability of **C$_8$SH** is thus higher than that of **Et$_3$-BTMT** although the latter forms at least twice as many thiol-gold bonds with the surface. This observation highlights that both chemisorptive (Au-S) bonding and vdW intermolecular interactions are (equally) important contributors to the stability of thiol-based monolayers.[12,53]

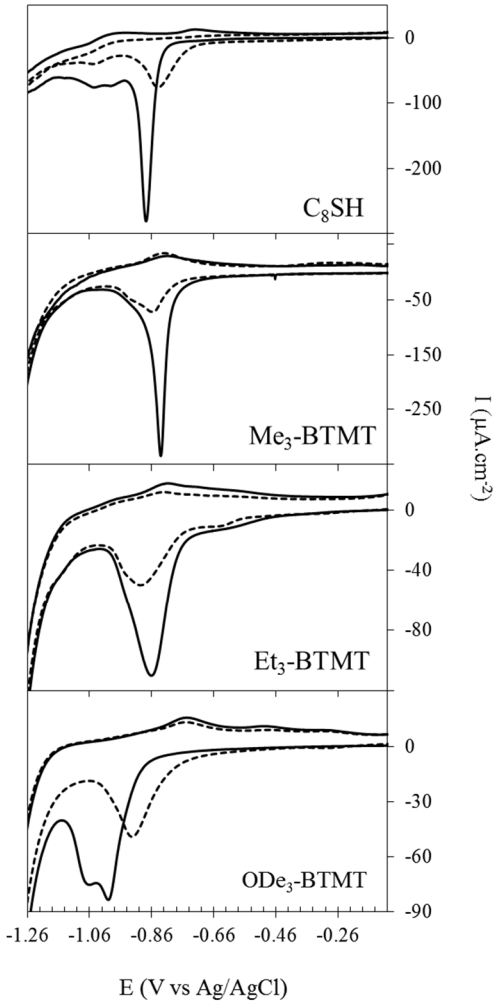

Fig. 7. Cyclic voltammograms of the reductive desorption of the four SAMs on gold working electrode in 0.5 M KOH. The first (solid line) and the second cycles (dashed line) are shown. Scan rate 0.02 V/s.

On the other hand, **C_8SH** and **Me_3-BTMT** show full width at half-maximum (fwhm) values of 37 mV and 46 mV respectively, while broader peaks are observed for **Et_3-BTMT** and **ODe_3-BTMT**, with fwhm of 113 and 124 mV respectively. A very small fwhm was previously explained by the extensive intermolecular interactions within the SAMs of n-alkanethiols. For aromatic trithiols SAMs, the relative sharpness of the reductive peak of **Me_3-BTMT** could be a confirmation of the suggested earlier standing up orientation of this molecule, which can engage in intermolecular π-interactions. On the other hand, the larger fwhm of **Et_3-BTMT** and **ODe_3-BTMT** is consistent with each adopting a lying down orientation on gold surface.

Integration of the reductive desorption peak of **C_8SH** yields a charge density (Q_c) of 33 µC/cm^2. This is smaller than theoretical value but consistent with other reports for gold surfaces prepared by analogous procedure (cleaning with piranha solution).[55,56] Electrochemical desorption of **Me_3-BTMT,**

Et_3-BTMT and **ODe_3-BTMT** is associated with the charge densities of 32 μC/cm^2, 24 μC/cm^2 and 15 μC/cm^2 respectively. The charge density was then converted to a surface concentration value assuming 1.3 electron per molecule for **Me_3-BTMT**, 2.2 for **Et_3-BTMT** and 2.7 for **ODe_3-BTMT** as per the XPS-derived ratios of bound to nonbound sulphur, Table 1. These calculations lead to surface concentrations of 3.6×10^{-10} mol/cm^2, 1.1×10^{-10} mol/cm^2 and 0.6×10^{-10} mol/cm^2, and molecular footprint areas of 0.7 nm^2, 1.6 nm^2 and 2.8 nm^2 for **Me_3-BTMT**, **Et_3-BTMT,** and **ODe_3-BTMT**, respectively. These values are in agreement with the XPS and STM data: as the size of the substituent increases the constituent molecules occupy a greater area in the respective SAMs.

In each of the four SAMs, upon reversing the scan direction, weak broad anodic (oxidation) peaks arise, characteristic of re-adsorption of the non-diffused thiolate. In the second CV cycle (Fig. 7, dashed curve), the oxidatively re-adsorbed thiols are again desorbed. Significant differences in the shape and position of the desorption peaks and in the quantity of reductive charges between the first and second cycle were observed, reflecting the change of the adsorbed state of the molecules.

For **C_8SH**, the integration of second reduction peak shows that 45% of the desorbed thiols molecules subsequently re-adsorb on an anodic scan. Similar redeposition efficiencies are measured for both **Me_3-BTMT** (44%) and **Et_3-BTMT** (49%). In contrast, **ODe_3-BTMT** undergoes much more extensive readsorption (95%). This is likely related to the lesser solubility of **ODe_3-BTMT** thiolate vs **Me_3-BTMT** and **Et_3-BTMT** in the aqueous electrolyte. Such behavior has been previously reported for **C_{16}SH** and explained by the formation of micelles of amphiphilic $C_{16}S^-$ at the electrode-electrolyte interface, which significantly lowers the diffusion coefficient.[57]

The reduction potential of the second voltammetric sweep undergoes a shift of +40 mV in the case of **C_8SH**, –20 mV for **Me_3-BTMT**, –30mV for **Et_3-BTMT**, and +80 mV for **ODe_3-BTMT**. This positive shift, frequently observed in alkanethiol desorption,[53,55] is attributed to the higher ionic permeability of the less ordered SAM that is formed during the oxidative readsorption. On the other hand, the formation of disulfide bridges between the free thiols of neighboring molecules within the SAM during the oxidative readsorption might explain the negative shift observed for **Me_3-BTMT** and **Et_3-BTMT.**[58,59]

Overall, the electrochemical data are thus consistent with a standing up organization of **Me_3-BTMT** and a lying down conformation of **Et_3-BTMT** and **ODe_3-BTMT**.[60] The standing up orientation yields a SAM with high molecular density, greater intermolecular interactions and the possibility of formation of a disulphide bonds. The lying down orientation of **ODe_3-BTMT** and to a lesser extent **Et_3-BTMT** (whose SAM also includes some standing-up molecules) yields a lower surface coverage and weaker intermolecular interactions.

CONCLUSIONS

A set of new tridentate molecules based on a benzene ring substituted with three methylthiol groups in alternation with three alkyl chains were synthesized and their self assembly on Au(111) was studied. STM characterization of the resulting SAMs revealed a locally ordered arrangement of bright protrusions attributable to individual molecules. XPS and electrochemistry results establish that the surface density and orientation of these molecules depend on the size of their substituents. SAMs of **Me_3-BTMT** exhibit the higher molecular density of the three molecules studied and the lowest ratio of bound/non-bound thiol. This suggests a preference for the standing-up orientation for this molecule. For **Et_3-BTMT**, the bulkier ethyl substituents favors a lying down orientation on the surface, yielding a SAM with a higher degree of chemisorption (>70% of thiol groups are bonded to gold). Finally, **ODe_3-BTMT**, predominantly adsorbs in a lying down orientation, with almost all its thiol groups bonded to the gold substrate. This orientation is driven mainly by the vdW interactions between the alkoxy chains and the gold, and between themselves. Overall, the balance between intermolecular and molecule–substrate interactions appear to determine the packing, orientation, and stability of the monolayer of tridentate thiols.

EXPERIMENTAL SECTION

Preparation of the SAMs. Au(111) substrates with atomically flat terraces were prepared by thermal evaporation of gold onto freshly cleaved mica sheets preheated at 450 °C under a pressure of 10^{-7}-10^{-8} Pa.[61] Au/Cr/glass and Au/Cr/Si substrates were purchased from Emtron Hybrids (Yaphank, NY).

The SAMs of **C_8SH**, **Me_3-BTMT, Et_3-BTMT** and **ODe_3-BTMT** SAMs were prepared by immersing the Au/mica (for STM measurements), Au/Cr/glass and Au/Cr/Si substrates (for other measurements) in a 0.1 mM DMF (ACS reagent) solution of the corresponding thiols under Ar atmosphere at room temperature for 18 hours. After SAM formation, the samples were thoroughly rinsed with pure DMF to remove physisorbed molecules and dried under a stream of ultrapure N_2.

Cyclic voltammetry (CV). Prior to SAM deposition, the gold electrodes were dipped into a freshly prepared piranha solution (concentrated H_2SO_4: 30% H_2O_2 = 3:1) for 5 min (caution: "piranha solution" reacts violently with organic materials and should be handled very carefully), rinsed with copious quantities of Milli-Q water, and dried under an N_2 stream. This was immediately followed by electrochemical polishing performed by repetitive CV cycles in 0.5 M H_2SO_4 solution from −0.4 to +1.5 V at 0.1 V/s, until reproducible voltammograms were obtained.

The electrode roughness factor γ was determined by integrating the charge of the reduction peak of the gold oxide.[62,63] Assuming a theoretical value[63] (Q_{O2}) of 400 μC/cm^2 for a monolayer of chemisorbed oxygen on a polycrystalline gold electrode and a geometric area (A_g) of the Au electrode of

3.2×10^{-3} cm^2, the Au electrode roughness factor was determined to be $\gamma = 1.3\pm 0.1$ ($\gamma = Qc/(A_g\times Q_{O2})$), where Qc is the charge of the reduction peak of gold oxide (μC)).

Cyclic voltammograms were acquired using a CHI 760C workstation (CH Instruments Inc, Austin, TX). The three-electrode electrochemical cell consisted of a modified Au electrode, a Pt wire counter electrode, and an Ag/AgCl reference electrode. The reductive desorption of the SAMs was performed in 0.5 M KOH solution, purged with high purity Ar for 15 min prior to measurements. The reductive desorption voltammograms were recorded by cycling the potential between 0.1 to −1.3 V at 0.02 V/s. The surface concentration of the adlayer, Γ_m (mol/cm^2) was obtained from Faraday's law: $\Gamma_m = Q/ZnFA$, where Q (μC) is the passed charge determined from the CVs by integrating the area under the reduction peak, Z is the number of electrons involved in the redox reaction, n is the number of moles of reactants, F is Faraday's constant and A is the active area of gold electrode ($A=Ag\times\gamma$ (cm^2)).

Scanning tunneling microscopy (STM). STM measurements were performed under ambient conditions using either a NanoSurf EasyScan 2 or Multimode8™ equipped with a Nanoscope™ V controller (Bruker, Santa Barbara, CA) and Nanoscope 8.15r3 software. The STM tips were mechanically cut from Pt/Ir wire (80/20, diameter 0.25 mm, Nanoscience). All STM-images were obtained in the constant current mode using an A scanner and low current STM converter by applying a tunneling current I_{set} of 70 to 250 pA and a sample bias V_{set} of 500 to 1400 mV. Calibration of the piezoelectric positioners was verified by atomic resolution imaging of graphite. The raw images were processed from WSxM5.0 software[64] through 2D-FFT and line profiles.

X-Ray photoelectron spectroscopy (XPS). XPS spectra were recorded on a ThermoFisher Scientific K-alpha instrument equipped with a monochromatic Al Kα X-ray source (1486.6 eV). Spectral energies were calibrated by setting the binding energy of Au $4f_{7/2}$ (84.0 eV). The peak-fitting procedure was performed using the Thermo Avantage software (version 4.60).

Supporting Information. Synthetic procedure and ^1H, ^{13}C NMR and MS characterization of **Me_3-BTMT, Et_3-BTMT, ODe_3-BTMT** and **ODe_3-B**. STM images of 1-octanethiol, approximate molecular dimensions of **Me_3-BTMT** and **Et_3-BTMT**, DFT calculated rotational itinerary for **Et_3-BTMT** and pair correlation analysis of the nearest three-point contacts for **Me_3-BTMT**, **Et_3-BTMT** and **ODe_3-BTMT.**

Corresponding Author

Bruce.Lennox@mcgill.ca; Dmitrii.Perepichka@mcgill.ca.

Present Addresses

† Polymer Source Inc., 124 Avro str., Dorval (Quebec) H9P 2X8 Canada.

‡ Division of Molecular Imaging and Photonics, Department of Chemistry, KU Leuven – University of Leuven, Celestijnenlaan 200 F, B-3001, Leuven, Belgium.

ACKNOWLEDGMENT

This work was financially supported by FQRNT (Quebec) and NSERC (Canada). M.A.M. thanks NSERC and FQRNT for doctoral fellowships. I.I.P. acknowledges FQRNT for a Postdoctoral Fellowship.

REFERENCES

1 J. Scherer, M. R. Vogt, O. M. Magnussen and R. J. Behm, *Langmuir*, 1997, **13**, 7045−7051.
2 H. Song, M. A. Reed and T. Lee, *Adv. Mater*., 2011, **23**, 1583− 1608.
3 B. De Boer, H. Meng, D. F. Perepichka, J. Zheng, M. M. Frank, Y. J. Chabal and Z. Bao, *Langmuir,* 2003, **19**, 4272–4284.
4 M. Halik and A. Hirsch, *Adv. Mater*., 2011, **23**, 2689−2695.
5 Arramel, T. C. Pijper, T. Kudernac, N. Katsonis, M. van der Maas, B. L. Feringa and B. J. van Wees, *Nanoscale*, 2013, **5**, 9277−9282.
6 A. P. Masillamani, S. Osella, A. Liscio, O. Fenwick, F. Reinders, M. Mayor, V. Palermo, J. Cornil and P. Samori, *Nanoscale*, 2014, **6**, 8969–8977.
7 L. Deng, M. Mrksich and G. M. Whitesides, *J. Am. Chem. Soc.,* 1996, **118**, 5136–5137.
8 J. J. Gooding, F. Mearns, W. Yang and J. Liu, *Electroanalysis*, 2003, **15**, 81–96.
9 V. Tabard-Cossa, M. Godin, I. J. Burgess, T. Monga, R. B. Lennox and P. Grütter, *Anal. Chem.,* 2007, **79**, 8136–8143.
10 N. K. Chaki and K. Vijayamohanan, *Biosens. Bioelectron*., 2002, **17**, 1−12.
11 C. Vericat, M. E. Vela, G. Benitez, P. Carro and R. C. Salvarezza, *Chem. Soc. Rev.,* 2010, **39**, 1805–1834.
12 J. C. Love, L. A. Estroff, J. K. Kriebel, R. G. Nuzzo and G. M. Whitesides, *Chem. Rev.,* 2005, **105**, 1103–1170.
13 R. G. Nuzzo, B. R. Zegarski and L. H. Dubois, *J. Am. Chem. Soc*., 1987, **109**, 733−740.
14 J. B. Schlenoff, M. Li and H. Ly, *J. Am. Chem. Soc*., 1995, **117**, 12528−12536.
15 M. H. Schoenfisch and J. E. Pemberton, *J. Am. Chem. Soc*., 1998, **120**, 4501–4513.
16 P. Chinwangso, A. C. Jamison and T. R. Lee, *Acc. Chem. Res.,* 2011, **44**, 511−519.
17 M. S. Miller, R. R. San Juan, M.-A. Ferrato and T .B. Carmichael, *J. Am. Chem. Soc*., 2013, **136**, 4212–4222.
18 J. K. Whitesell and H. K. Chang, *Science,* 1993, **261**, 73–76.
19 Y. Yao and J. M. Tour, *J. Org. Chem.,* 1999, **64**, 1968–1971.
20 H. Jian and J. M. Tour, *J. Org. Chem.,* 2003, **68**, 5091–5103.
21 J. –S. Park, A. N. Vo, D. Barriet, Y. –S. Shon and T. R. Lee, *Langmuir,* 2005, **21**, 2902–2911.
22 T. Kitagawa, Y Idomoto, H. Matsubara, D. Hobara, T. Kakiuchi, T. Okazaki and K. Komatsu, *J. Org. Chem.,* 2006, **71**, 1362−1369.
23 S. Katano, Y. Kim, H. Matsubara, T. Kitagawa and M. Kawai, *J. Am. Chem. Soc.,* 2007, **129**, 2511–2515.
24 B. Singhana, S. Rittikulsittichai and T. R. Lee, *Langmuir,* 2013, **29**, 561−569.
25 B. Singhana, A. C. Jamison, J. Hoang and T. R. Lee, *Langmuir,* 2013, **29**, 14108−14116.
26 J. E. Hutchison, T. A. Postlethwaite and R. W. Murray, *Langmuir*, 1993, **9**, 3277–3283.
27 E. U. Thoden van Velzen, J. F. J. Engbersen, P. J. de Lange, J. W. G. Mahy and D. N. Reinhoudt, *J. Am. Chem. Soc.,* 1995, **117**, 6853–6862
28 L. Zhu, H. Tang, Y. Harima, K. Yamashita, D. Hirayama, Y. Aso and T. Otsubo, *Chem. Commun*., 2001, 1830–1831.
29 L. Wei, H. Tiznado, G. Liu, K. Padmaja, J. S. Lindsey, F. Zaera and D. F. Bocian, *J. Phys. Chem. B.,* 2005, **109**, 23963–23971.
30 Y. Shirai, L. Cheng, B. Chen and J. M. Tour, *J. Am. Chem. Soc.,* 2006, **128**, 13479–13489.
31 T. Kitagawa, H. Matsubara, K. Komatsu, K. Hirai, T. Okazaki and T. Hase, *Langmuir,* 2013, **29**, 4275–4282.
32 M. A. Fox, J. K. Whitesell and A. J. McKerrow, *Langmuir,* 1998, **14**, 816–820.
33 N. Phares, R. J. White and K. W. Plaxco, *Anal. Chem*., 2009, **81**, 1095–1100.

34 A. A. Yasseri, D. Syomin, V. L. Malinovskii, R. S. Loewe, J. S. Lindsey, F. Zaera and D. F. Bocian, *J. Am. Chem. Soc*., 2004, **126**, 11944−11953.
35 A. M. Moore, A. A. Dameron, B. A. Mantooth, R. K. Smith, D. J. Fuchs, J. W. Ciszek, F. Maya, Y. Yao, J. M. Tour and P. S. Weiss, *Langmuir,* 1998, **14**, 816−820.
36 K. Shimazu, M. Takechi, H. Fujii, M. Suzuki, H. Saiki, T. Yoshimura and K. Uosaki, *Thin Solid Films*, 1996, **273**, 250−253.
37 S. Watcharinyanon, C. Puglia, E. Gothelid, J. E. Backvall, E. Moons and L. S. O. Johansson, *Surf. Sci*., 2009, **603**, 1026–1033.
38 G. Hennrich and E. V. Anslyn, *Chem. Eur. J.,* 2002, **8**, 2218–2224.
39 J. A. Burns and G. M. Whitesides, *J. Am. Chem. Soc.,* 1990, **112**, 6296–6303.
40 K. S. Mali, J. Adisoejoso, E. Ghijsens , I. De Cat and S. De Feyter, *Acc. Chem. Res*., 2012, **45** 1309–1320.
41 A. Ciesielski, C. A. Palma, M. Bonini and P. Samorì, *Adv. Mater.,* 2010, **22**, 3506–3520.
42 Y. Xue and M. B. Zimmt, *J. Am. Chem. Soc*., 2012, **134**, 4513–4516.
43 M. G. Sarwar, B. Dragisic, S. Sagoo and M. S. Taylor, *Angew. Chem. Int. Ed.,* 2010, **49**, 1674–1677.
44 A. C. Sather, O. B. Berryman and J. Rebek Jr, *J. Am. Chem. Soc.,* 2010, **132**, 13572–13574.
45 X. Wang and F. Hof, *Beilstein J. Org. Chem.,* 2012, **8**, 1–10.
46 G. E. Poirier, *Chem. Rev.,* 1997, **97**, 1117–1128.
47 J. E. Martin, J. P. Wilcoxon, J. Odinek and P. Provencio, *J. Phys. Chem. B*, 2000,**104**, 9475–9486.
48 L. R. Merte, R. Bechstein, G. W. Peng, F. Rieboldt, C. A. Farberow, H. Zeuthen, J. Knudsen, E. Laegsgaard, S. Wendt, M. Mavrikakis and F. Besenbacher. *Nat. Commun*., 2014, **5**, 4193.
49 K. Tahara, S. Lei, J. Adisoejoso, S. De Feyter and Y. Tobe, *Chem. Commun.,* 2010, **46**, 8507–8525.
50 D. G. Castner, K. Hinds and D. W. Grainger, *Langmuir,* 1996, **12**, 5083−5086.
51 C. D. Bain, J. Evall and G. M. Whitesides, *J. Am. Chem. Soc.,* 1989, **111**, 7155–7164.
52 C. A. Widrig, C. Chung and M. D. Porter, *J. Electroanal. Chem*., 1991, **310**, 335–359.
53 T. Kakiuchi, H. Usui, D. Hobara and M. Yamamoto, *Langmuir,* 2002, **18***,* 5231–5238.
54 Y.-F. Liu and Y.-L. Lee, *Nanoscale*, 2012, **4**, 2093–2100.
55 F. Feng, T. Niu, X. You, Z. Wan, Q. Kong and S. Bi, *Analyst,* 2011, **136**, 5058–5063.
56 J. Tkac and J. J. Davis, *J. Electroanal. Chem*., 2008, **621**, 117–120.
57 D. F. Yang, C. P. Wilde and M. Morin, *Langmuir,* 1997, **13***,* 243–249.
58 S. Rifai and M. Morin, *J. Electroanal. Chem.,* 2003, **550**, 277–289.
59 F. P. Cometto, C. A. Calderón, E. M. Euti, D. K. Jacquelín, M. A. Pérez, E. M. Patrito and V. A. Macagno, *J. Electroanal. Chem*., 2011, **661**, 90–99.
60 Ellipsometric measurements are in agreement with the suggested structure of the SAMs, yielding film thickness of 0.8 ± 0.4 nm for Et_3-BTMT and 1.1 ± 0.3 nm for Me_3-BTMT, although the observed (and expected) differences are smaller than the uncertainty of the method.
61 M. H. Dishner, M. M. Ivey, S. Gorer, J. C. Hemminger and F. J. Feher, *J. Vac. Sci. Technol.* A., 1998, **16**, 3295–3300.
62 J. C. Hoogvliet, M. Dijksma, B. Kamp and W. P. Van Bennekom, *Anal. Chem.,* 2000, **72**, 2016–2021.
63 S. Trasatti and O. A. Petrii, *Pure & Appl. Chem.,* 1991, **63**, 711–734.
64 I. Horcas, R. Fernandez, J. M. Gomez-Rodriguez, J. Colchero, J.; Gomez-Herrero and A. Baro, *Rev. Sci. Instrum.,* 2007, **78**, 1–8.

TOC graphics: